Jurnal Kejuruteraan 37(6) 2025: 2829-2840
https://doi.org/10.17576/jkukm-2025-37(6)-21

An Enhanced Symmetrized Implicit Trapezoidal Rule for Dampening the Oscillatory Behaviour of Numerical Solutions

Noorhelyna Razali[a], Noor Farah Wahida Abdul Rashid[a*], Nisa Balqis[a], Mansor[b], Khew Ho Yuan[b], Izamarlina Asshaari[a], Shahrum Abdullah[a] & Firdaus Mohamad Hamzah[c]

[a]*Faculty of Engineering and Built Environment, Universiti Kebangsaan Malaysia*

[b]*Centre of Excellence Complex, Proton Holding Berhad*

[c]*Centre for Defense Foundation Studies, Universiti Pertahanan Nasional Malaysia*

**Corresponding author: nfwahida2023@gmail.com*

Received 1 November 2024, Received in revised form 10 June 2025
Accepted 10 July 2025, Available online 30 September 2025

ABSTRACT

The symmetrized implicit trapezoidal rule (SITR) is a novel finite difference method that involves symmetrization of the calculated numerical solutions using the implicit trapezoidal rule (ITR). By solving differential equations using large space and time steps, compared with conventional methods, the SITR method can generate more accurate results by preventing oscillations in the numerical solutions. In this study, the effect of parameters such as the space step and time step on the accuracy and computational efficiency of the active one-step symmetrized implicit trapezoidal rule (1SITR), the active two-step symmetrized implicit trapezoidal rule (2SITR) and the generalized trapezoidal differencing time-marching (GTDTM) method is investigated in solving aeroacoustics problem involving a linear advection equation. The results of the study show that compared to the conventional GTDTM method, both the enhanced 1SITR and 2SITR methods possess damping characteristics that reduce the oscillatory behaviour of the numerical solution, leading to better solution accuracy at large spatial and temporal step sizes. At smaller temporal step sizes, the increase in the dissipative characteristics of 1SITR and 2SITR reduces their accuracy. The computational time for both 1SITR and 2SITR is greater than that for GTDTM due to the extra symmetrization calculations. This study presents a unique contribution through the development of two symmetrized implicit trapezoidal rule methods which provide improved damping characteristics, allowing for more stable and accurate solutions even under coarse discretization settings.

Keywords: Numerical method; finite difference method; acoustic analysis; symmetrization; implicit trapezoidal rule

INTRODUCTION

Numerical methods are widely employed in solving scientific and engineering problems. With advancements in digital technology, engineering problems are becoming more complex and less efficient. On the other hand, numerical methods have become more advanced and have many advantages compared to analytical methods including high computational speed, low computational cost, and ease of parameter manipulation in numerical experiments (Hakroa et al. 2024; Ismail & Azadbakht 2024). The selection of a numerical method often depends on the requirements of the problem and researchers. The finite difference (FD) method is one of the most popular choices for the analysis of acoustics due to its versatility and stability (Simillides et al. 2024).

Despite all the advantages of FD methods, because of the approximation of continuous mathematical models, discretization errors are inevitable. This leads to a decrease in the accuracy of the computed numerical solution. To date, many studies have been conducted to develop and test new FD schemes to improve accuracy and computational efficiency. One common approach is to develop higher-order FD schemes. For instance, Ranocha (2018) demonstrated the strong stability of the fourth-order ten-stage RK method presented by (Ketcheson, 2008) which can be implemented in an efficient low-storage form with a rational FD coefficient. E. Wang & Liu (2019) developed an explicit FD scheme with arbitrary even-order accuracy in space and fourth- and sixth-order accuracy in time based on a general cuboid stencil for modelling 3D wave equations. Furthermore, some studies have focused on developing new stencils to increase the accuracy of FD schemes (Liu & Sen 2013; Z. Wang & Chen 2018; Xu & Liu, 2018) while other studies have included optimization to obtain optimal FD coefficients (Boom & Zingg, 2018; Rona & Pirozzoli, 2017; Simillides et al. 2024; Xu & Liu, 2018; Yang & Liu, 2016, 2017) to maximize approximation accuracy regardless of wavenumber. Several researchers have enhanced the accuracy of the FD method on staggered grids, which are more flexible than conventional squares and equal spacing grids along different axial directions (H. Chen & Chen, 2017; Y. Chen & Deng, 2019; Ren & Sen, 2017; Tan & Huang, 2014). Another common approach for achieving high accuracy in FD methods is to use implicit or compact FD schemes. The adoption of implicit FD schemes involves solving a set of linear equations that can be transformed into a multidiagonal matrix system (Lele, 1992). Implicit or compact FD schemes can yield higher spatial resolution, as rational expansion usually converges faster than power series expansion (Kosloff D. Tal-Ezer, 2010; Lele, 1992; Zhou & Ortigosa, 2008). However, large matrix systems usually require large amounts of computational memory and hence, high computational costs in addition to reduced computational efficiency. For these reasons, previous related studies have usually focused on developing efficient inversion methods for matrix systems. These include prefactorization of the matrix system by Zhou & Zhang (2011) and splitting algorithms that transform a multidiagonal matrix into individual tridiagonal matrices for easier inversion processes (Nunez & Rao 2013; Rona & Pirozzoli 2017; Zhang & Lu 2007). In another approach, Francesca & Muhieldeen (2020) investigated the effect of the combination of explicit and implicit factors on the accuracy and computational efficiency of an implicit FD scheme.

Another approach to increase the accuracy of an FD scheme is symmetrization, which compared with other approaches is less explored. This method is based on a smoothing technique for arbitrary symmetric Runge–Kutta methods generalized by Chan & Gorgey (2013). In an experimental study by Chan & Razali(2014); Razali et al.(2018); Razali & Chan (2015), practical execution of smoothing technique was conducted for solving stiff problems and these methods can avoid order reduction problems. Even though finite difference methods (FDM) are frequently used to solve wave equations, they frequently have spurious oscillations and numerical dispersion, especially when advection-dominated issues are involved. These limitations affect the accuracy and stability of the numerical solutions, particularly when longer time steps are applied.

Recent research has focused on specific issues related to stability maintenance and the accuracy of wave propagation. Zhang et al. (2021) introduced high-order implicit-explicit Runge–Kutta methods that uphold both the maximum principle and energy stability, especially for space-fractional Allen–Cahn equations. Additionally, Chen et al. (2023) created a compact high-order finite-difference scheme with optimized coefficients specifically designed for the 2D acoustic wave equation, resulting in improved computational efficiency and accuracy. At the same time, Chang et al. (2023) presented a 2.5D generalized finite-difference method that simplifies 3D elastic wave problems into a series of 2D computations, thereby significantly boosting accuracy and lowering computational costs. These findings underscore the rapid evolution of FD-based methods to address the increasing complexity of contemporary wave propagation issues.

In this paper, a new symmetrized method is constructed by analyzing the order and damping conditions in Implicit Trazepoidal Rule (ITR). The method is applied in active mode where symmetrization is applied at every steps. The new methods are applied to solve the linear advection equation. The obtained results are compared to those of the conventional generalized trapezoidal differencing time-marching (GTDTM) method by Francesca & Muhieldeen (2020). This paper aims to investigate the effect of step size and the differences in computational accuracy and efficiency among the three studied methods.

METHODOLOGY

The new method is constructed such that it preserved the symmetry property of the numerical method by analysing the order conditions and damping conditions. This process is called symmetrization where the asymptotic error expansion in the even powers of the step size is preserved. The coding for each method is established in MATLAB and is checked for errors. After the verification step, the selected benchmark problem from Computational Aeroacoustics (CAA) Workshop on Benchmark Problems by Dahl (2000) is chosen to test the performance of studied

FD methods The computation steps are repeated for each studied method. The consistency of the generated results is checked to detect problems in the codes. If the results are free from abnormalities, then the performance of 1SITR and 2SITR in solving the benchmark problem is investigated. The use of symmetrized implicit schemes such as 1SITR and 2SITR has recently demonstrated improvements in both temporal precision and damping management in simulations of wave propagation (Gao et al. 2025). These methods preserve energy stability over long-time integration, making them particularly suitable for aeroacoustic problems (Hong et al. 2022). The process involves the determination of the average error and computation time for each method which is discussed in detail in the Results and Discussion.

NUMERICAL METHOD

An s-stage Runge–Kutta method with stepsize h for the step is a one-step method defined by

$$Y_i = y_{n-1} + h \sum_{j=1}^{s} a_{ij} f(x_{n-1} + c_j h, Y_j), \tag{1}$$

$$y_n = y_{n-1} + h \sum_{i=1}^{s} b_i f(x_{n-1} + c_i h, Y_i) \tag{2}$$

where A is an $s{\times}s$ Runge–Kutta matrix, b and c are $s{\times}1$ vectors of weights and abscissas respectively and be denoted by $R{=}(A,b,c)$. The implicit trapezoidal rule is a 2-stage method with Butcher tableau

$$\begin{array}{c|cc} 0 & 0 & 0 \\ 1 & \frac{1}{2} & \frac{1}{2} \\ \hline & \frac{1}{2} & \frac{1}{2} \end{array} \tag{3}$$

and defining equation

$$\begin{aligned} Y_1 &= y_{n-1} \\ Y_2 &= y_{n-1} + \frac{h}{2}(f(x_{n-1}, Y_1) + \mathrm{f}(x_n, Y_2) \\ y_n &= y_{n-1} + \frac{h}{2}(f(x_{n-1}, Y_1) + f(x_n, Y_2) \\ &= Y_2 \end{aligned} \tag{4}$$

The new enhanced numerical method is constructed to reduce the oscillatory behaviour in the numerical solution and to suppress order reduction when solving stiff numerical problems. The method is called symmetric or self-adjoint if $-R^{-1}{=}R$. An algebraic characteristic of a symmetric method is given by $PAP + A = eb^{\mathsf{T}}$, $Pb{=}b$, $Pc = e - c$. The one-step symmetrizer must satisfy the symmetry property and thus the Butcher table for the one-step symmetrizer is obtained as follows:

$$\begin{array}{c|c} \tilde{c} & \tilde{A} \\ \hline & \tilde{b}^{\cdot} \end{array} = \begin{array}{c|cc} c & A & 0 \\ e+c & eb^{\cdot} & A \\ \hline & b^{\cdot} - u^{\cdot} P & u^{\cdot} \end{array} \tag{5}$$

where A is an $s \times s$ Runge–Kutta matrix, b and c are $s \times 1$ vectors of weights and abscissas, respectively, P is the permutation matrix, and u is chosen to satisfy the damping and order conditions. Note that one-step symmetrization is a composition of two symmetric methods with appropriate weights. The Butcher tableau for ITR and enhanced one-step method (1SITR) is shown in Equation (6):

$$\begin{array}{c|ccc} 0 & 0 & 0 & 0 \\ 1 & \frac{1}{2} & \frac{1}{2} & 0 \\ 2 & \frac{1}{2} & 1 & \frac{1}{2} \\ \hline & \frac{3}{8} & \frac{1}{2} & \frac{1}{8} \end{array} \tag{6}$$

The stability function of a Runge–Kutta method with coefficients $(A,\ b,\ c)$ is defined by

$$R(z) = 1 + zb^{\mathsf{T}}(I - zA)^{-1}e. \tag{7}$$

Equation (7) evaluates the numerical stability of the scheme across different discretization parameters. A method is considered stable if the stability function satisfies $|R(z)|\leq 1$.

Using the matrix given in equation (7), the stability function of 1SITR is as follow:

$$R(z) = \frac{1}{\left(1 - \frac{z}{2}\right)^2} \tag{8}$$

This method possesses damping characteristics such as $R(z) \to \frac{8}{z^2}$ when $z\to\infty$. The second-order behaviour is retained as the local error is damped by R(z). The update equation of 1SITR is given by the following:

$$\hat{u}_n = \frac{u_{n-1} + 2u_n + u_{n+1}}{4} \tag{9}$$

where $\hat{u}_n$ is the symmetrized value. This value at the nth step is calculated by reference to the n – 1*th* and n + 1*th* values. The Butcher tableau for the two-step symmetrizer is given as follows:

$$\begin{array}{c|cccc} c & A & 0 & 0 & 0 \\ e+c & eb^{\intercal} & A & 0 & 0 \\ 2e+c & eb^{\intercal} & eb^{\intercal} & A & 0 \\ 3e+c & eb^{\intercal} & eb^{\intercal} & eb^{\intercal} & A \\ \hline & b^{\intercal}-v^{\intercal}P & b^{\intercal}-u^{\intercal}P & u^{\intercal} & v^{\intercal} \end{array} \tag{10}$$

The weight vectors *u* and *v* are chosen to satisfy the damping and order conditions. The Butcher tableau for 2SITR is shown in Equation (11) as follows:

$$\begin{array}{c|ccccc} 0 & 0 & 0 & 0 & 0 & 0 \\ 1 & \frac{1}{2} & \frac{1}{2} & 0 & 0 & 0 \\ 2 & \frac{1}{2} & 1 & \frac{1}{2} & 0 & 0 \\ 3 & \frac{1}{2} & 1 & 1 & \frac{1}{2} & 0 \\ 4 & \frac{1}{2} & 1 & 1 & 1 & \frac{1}{2} \\ \hline & \frac{17}{32} & \frac{15}{16} & \frac{1}{2} & \frac{1}{16} & \frac{-1}{32} \end{array} \tag{11}$$

The stability function of the 2SITR is given by Equation (12) as follows:

$$R(z) = \frac{1 - \frac{z^2}{2}}{\left(1 - \frac{z}{2}\right)^4} \tag{12}$$

The method also possesses damping characteristics because $R(z) \to \frac{8}{z^2}$ when z→∞. Second-order behaviour is also retained for a similar reason. The update equation of 2SITR is given by Equation (13).

$$\hat{u}_n = \frac{-u_{n-2} + 4u_{n-1} + 10u_n + 4u_{n+1} - u_{n+2}}{16} \tag{13}$$

The symmetrized value, $\hat{u}_n$, is calculated by referring to the values between the *n–2nd* and *n+2nd* values.

DISCRETIZATION EQUATION

The chosen benchmark problem is the 1-D linear advection equation, as shown in Equation (14) as follows:

$$\frac{\partial u}{\partial t} + \frac{\partial u}{\partial x} = 0 \tag{14}$$

where *u* is wave amplitude, *t* is time parameter and *x* is space parameter. The initial condition of the chosen initial value problem is shown in equation (15)

$$u(x,0) = 0.5\, exp\left[-\, ln(2)\left(\frac{x}{3}\right)^2\right] \tag{15}$$

Equation (16) provides exact solution of linear advection equation.

$$u(x,t) = 0.5\, exp\left[-\, ln(2)\left(\frac{x-t}{3}\right)^2\right] \tag{16}$$

From equation (14), discretization to ITR obtained

$$\frac{u_j^{n+1} - u_j^n}{dt} = \frac{c}{2}\left[\frac{u_{j+1}^{n+1} - u_{j-1}^{n+1}}{2dx} + \frac{u_{j+1}^n - u_{j-1}^n}{2dx}\right] \tag{17}$$

where *n* is the time index, *j* is the space index along *x*-axis, *c* is a constant that represent fluid velocity, *dt* is the time step and *dx* is the space step. Equation (17) can be rearranged and represented as shown in Equation (18) as follows:

$$\begin{aligned} &\frac{r}{4}u_{j-1}^{n+1} + u_j^{n+1} - \frac{r}{4}u_{j+1}^{n+1} \\ &= -\frac{r}{4}u_{j-1}^n + u_j^n + \frac{r}{4}u_{j+1}^n \end{aligned} \tag{18}$$

where

$$r = -\frac{dt}{dx} \tag{19}$$

Here, the constant *r* is used to denote the Courant number and is given by Equation (19) after deriving from Equation (14). Because of the need to solve Equation (18) at every time and space step, a system of linear equations is formed and can be transformed into matrix form, as shown in Equation (20):

$$\begin{bmatrix} 1 & -\frac{r}{4} & \ddots \end{bmatrix} [u_1^{n+1} \quad \vdots \quad u_k^{n+1}] = \begin{bmatrix} 1 & \frac{r}{4} & \ddots \end{bmatrix} \tag{20}$$

In a general representation, the matrix Equation (20) can be written as:

$$M_L U^{n+1} = M_R U^n \tag{21}$$

or

$$U^{n+1} = M_L U^{-1} \cdot (M_R U^n) \tag{22}$$

where M_L and M_R is the left and right coefficient matrix of the equation while U_{n+1} and U_n is the column matrix that contain the updated values for every node in the space domain at present and future time. The computation of the discretized equations involves the inversion of matrix M_L and is done using MATLAB program.

NUMERICAL PERFORMANCE

The numerical performance of the three studied FD methods, namely, 1SITR, 2SITR and GTDTM is measured in terms of the accuracy of the solution and the duration of the computation. The accuracy of the FD methods is determined by calculating the average error, $\bar{\varepsilon}_n$, between the numerical solution and the exact solution as shown in Equation (23) determined by (Francesca & Muhieldeen, 2020):

$$\bar{\varepsilon}_n = \frac{1}{n}\sum_{i=1}^{n} |\bar{u}_i - u_i| \tag{23}$$

where $\bar{u}$ is the exact value of the wave amplitude and u is the value of the wave amplitude calculated numerically. A plot of $\bar{\varepsilon}_n$ against *dt* at different *dx* values is generated to provide a graphical view of the effect.

The spatial domain x∈[–20,100] and time domain t∈[0,60] were fixed throughout the study to reflect a consistent wave propagation interval. The step sizes *dx* and *dt* were selected empirically to balance computational efficiency and resolution, while allowing systematic observation of oscillation and dissipation effects across methods. As the 1SITR and 2SITR schemes are unconditionally stable, a range of step sizes was explored to evaluate the stability limits and damping behaviour of the proposed methods in comparison to GTDTM. This approach enables a fair assessment of performance under both coarse and refined discretizations.

To assess the accuracy of each numerical method, the average absolute error was computed and this error indicates the mean of the absolute differences between the numerical and exact solutions across the spatial domain. The computation time for each FD method was also recorded in MATLAB and tabulated. The procedure was performed by the built-in stopwatch function of the program. To obtain accurate computation time results, the codes for each method are run five times, and the results are averaged.

RESULTS AND DISCUSSION

COMPUTATIONAL ACCURACY

The solution curves for each method are generated at various space steps, *dx* and time steps, *dt*. Figures 1, 2 and 3 illustrate the solution curves of the solutions generated using GTDTM, 1SITR and 2SITR respectively, at large space steps (*dx*=1.2) and various time steps *dt*. At large space steps, both GTDTM and 2SITR showed oscillating solutions, while 1SITR avoids oscillation because of its stronger damping behaviour. As a result, 1SITR has the lowest average error at a larger dt. As *dt* is reduced, the oscillation in the calculated solution by GTDTM has virtually not decreased whereas the solution oscillation is reduced in the case of 2SITR which reduces its average error, as shown in Figure 9. In the event of *dt* reduction, 1SITR shows an increase in damping characteristics as well as dissipation problems which explains the dramatic increase in the average error. As *dt* decreases below 0.12, 1SITR becomes unstable.

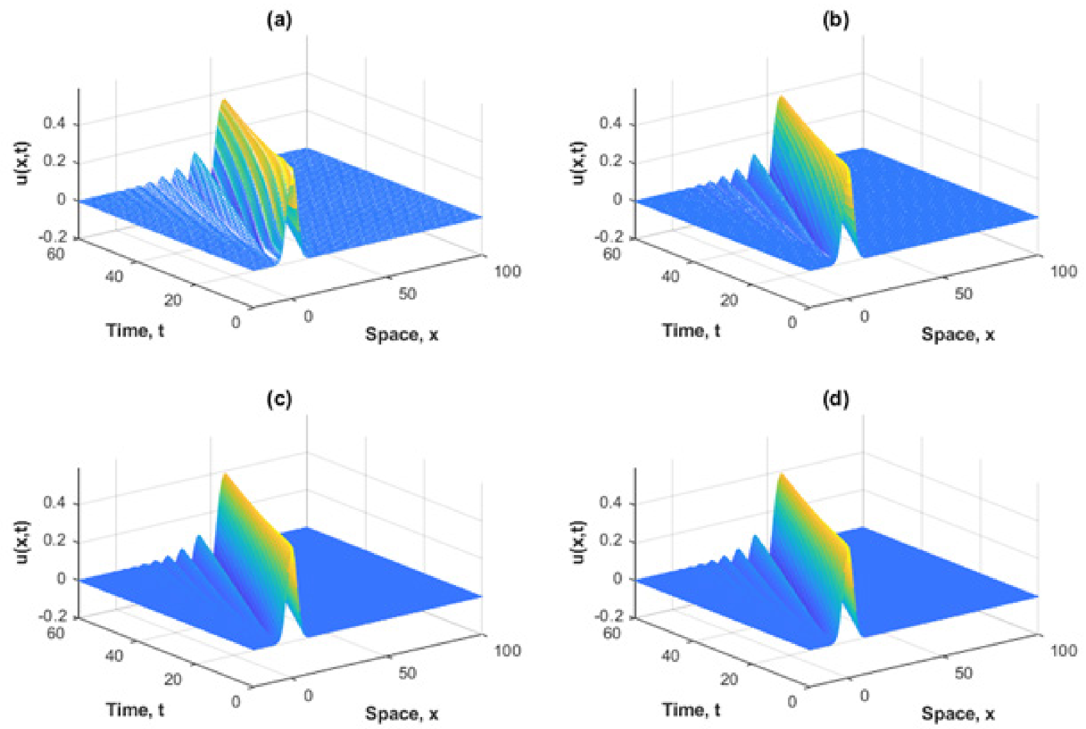

FIGURE 1. Solution curves for the GTDTM at fixed dx = 1.2 and varied dt: (a) dt = 1.2, (b)dt = 0.6, (c) dt = 0.12, and (d)dt = 0.24

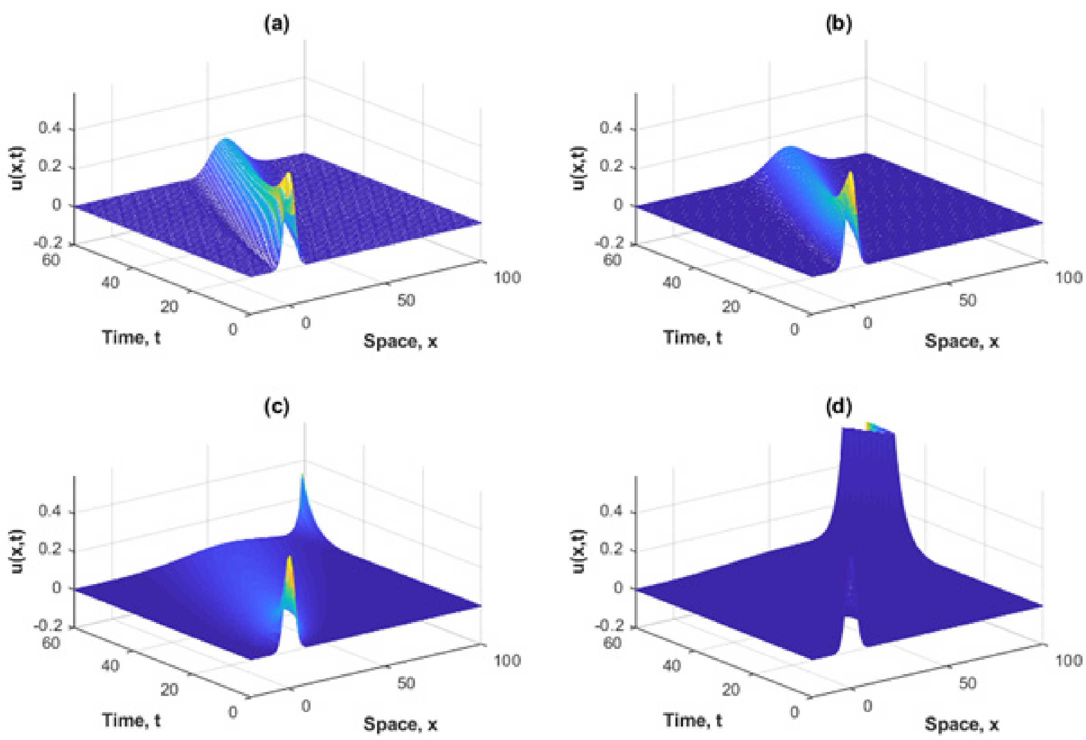

FIGURE 2. Solution curves for the 1SITR at fixed dx= 1.2 and varied dt: (a) dt = 1.2, (b) dt = 0.6, (c) dt = 0.12, and (d) dt = 0.24

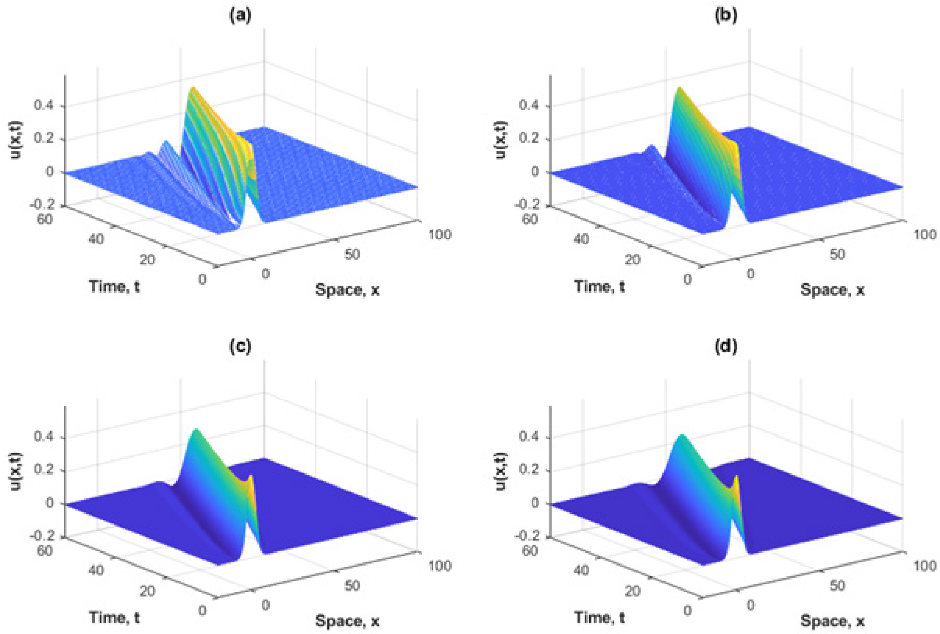

FIGURE 3. Solution curves for the 2SITR at fixed dx = 1.2 and varied dt: (a) dt = 1.2, (b) dt = 0.6, (c) dt = 0.12, and (d) dt = 0.24

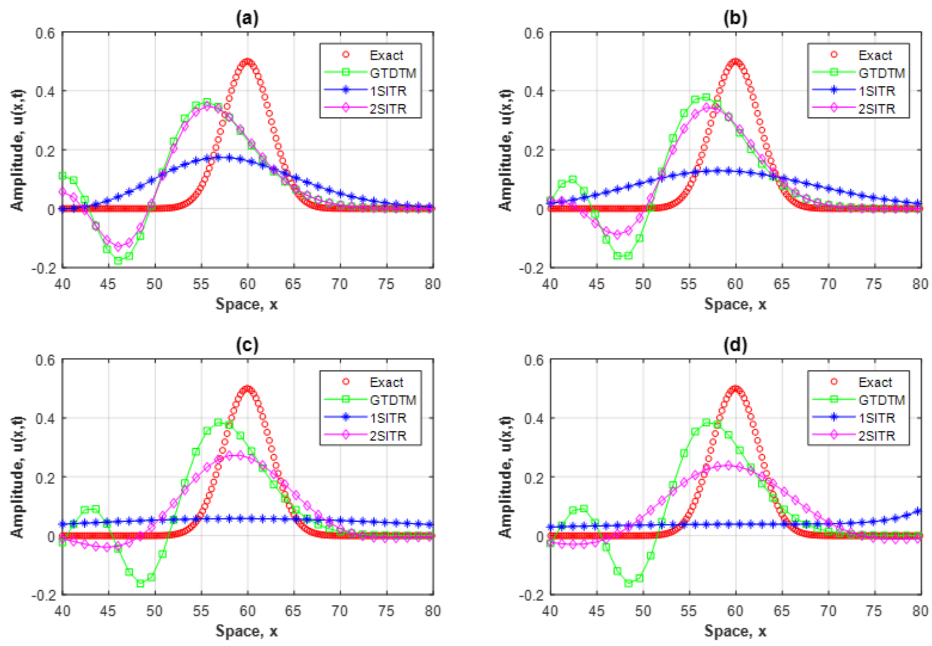

FIGURE 4. Amplitude of each method at dx = 1.2, t = 60 s and varied dt: (a) dt = 1.2, (b) dt = 0.6, (c) dt = 0.12, and (d) dt = 0.24

Figure 4 shows the amplitude, u calculated by each method at dx=1.2 and t=60 s. GTDTM exhibits visible oscillations and overshoots, particularly at large time steps, while images of the damping and dissipative behaviour of 1SITR and 2SITR reveal that an increase in dt results in greater damping of oscillations but also an increase in dissipation which may compromise the accuracy of the method. The damping and dissipative characteristics seen in the SITR methods suggest that a larger dt results in a greater reduction of oscillations. However, this increase also brings more dissipation, potentially affecting the precision of the numerical solution.

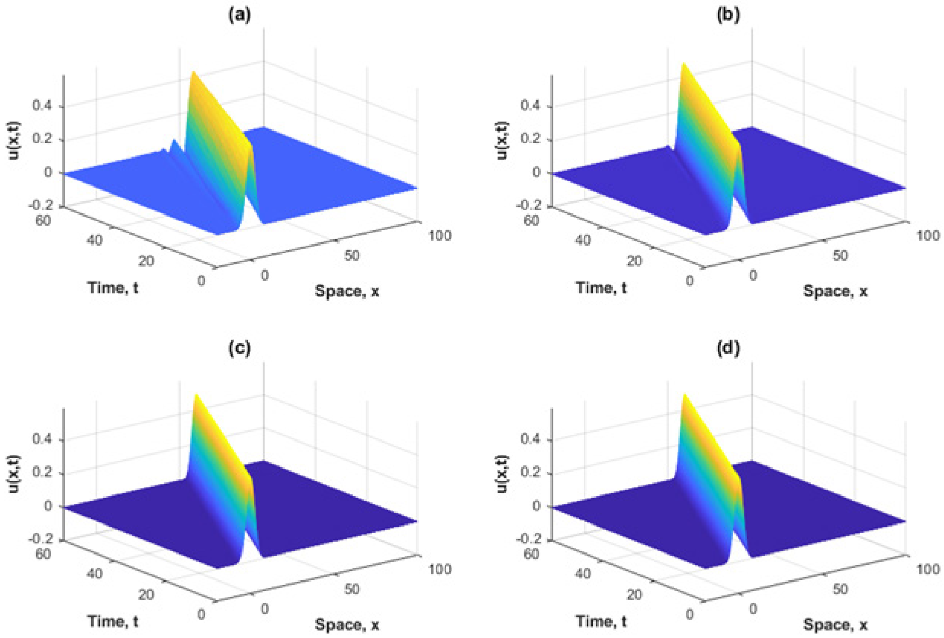

FIGURE 5. Solution curves for GTDTM at fixed *dx*= 0.24 and varied *dt*: (a) *dt* = 1.2, (b) *dt* = 0.6, (c) *dt* = 0.12, and (d) *dt* = 0.24

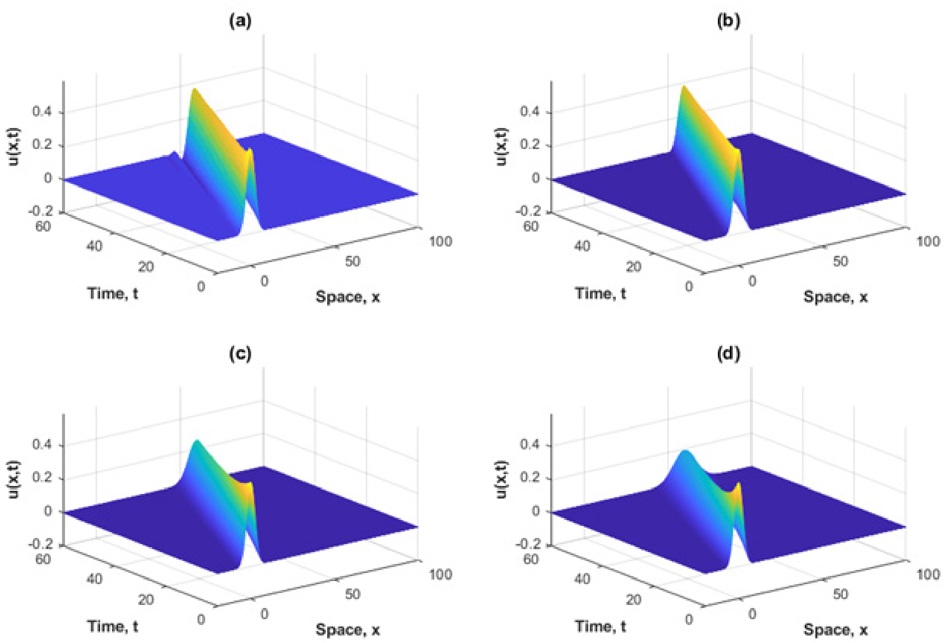

FIGURE 6. Solution curves for 1SITR at fixed *dx*= 0.24 and varied *dt*: (a) *dt* = 1.2, (b) *dt* = 0.6, (c) *dt* = 0.12, and (d) *dt* = 0.24

Figures 5, 6 and 7 illustrate the solution curves of the solutions generated using GTDTM, 1SITR and 2SITR respectively, at smaller space steps (*dx*=0.24) and various dt values. At a smaller space step, both GTDTM and 2SITR exhibit an oscillation in the calculated solution. This oscillation is prevented by reducing *dt*. As *dt* decreases, all methods show a decrease in average error in the calculated solution.

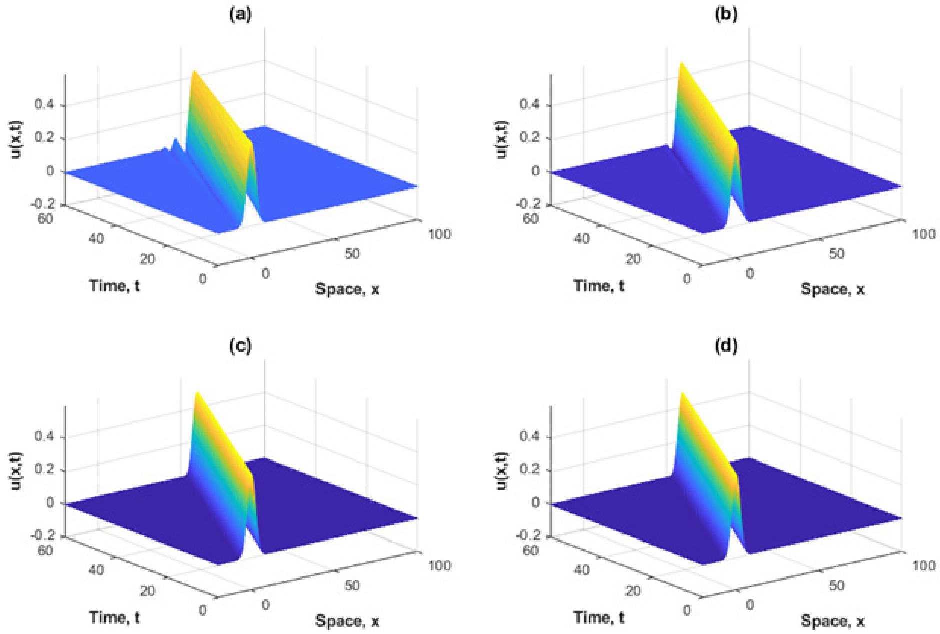

FIGURE 7. Solution curves for 2SITR at fixed *dx*= 0.24 and varied *dt*: (a) *dt* = 1.2, (b) *dt* = 0.6, (c) *dt* = 0.12, and (d) *dt* = 0.24

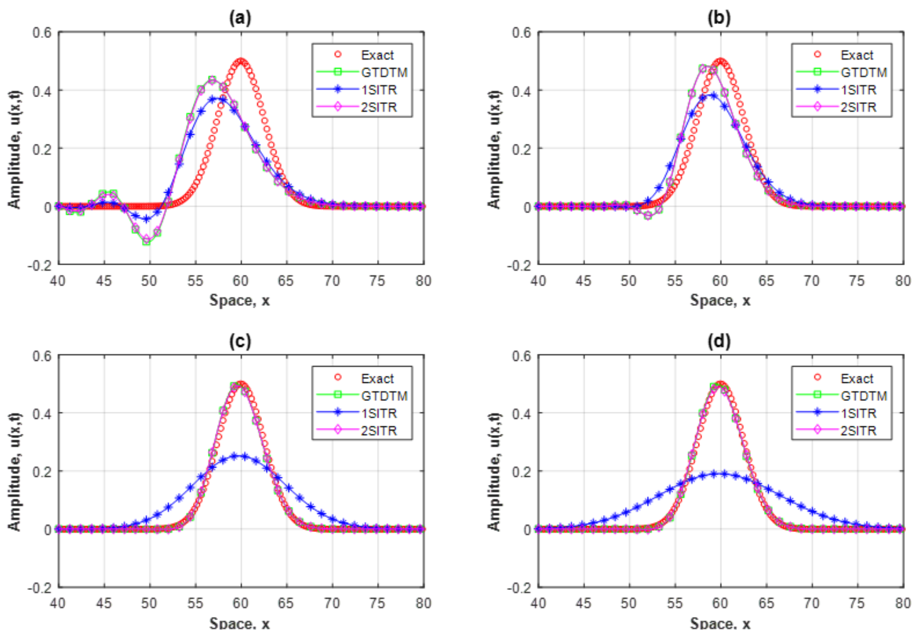

FIGURE 8. Amplitude of each method at *dx* = 0.24,*t* = 60 s and varied *dt*: (a) *dt* = 1.2, (b) *dt* = 0.6, (c) *dt* = 0.12, and (d) *dt* = 0.24

Figure 8 shows the amplitude, *u* calculated by each method at *dx*= 0.24 and *t*=60s. Similar to the case when *dx*=1.2, an increase in *dt* not only results in higher damping of oscillation but also an increase in dissipation. From (a) to (c), a reduction in *dt* leads to enhanced accuracy across all methods, as GTDTM progressively diminishes oscillatory behavior while SITR methods continue to preserve smooth profiles. Meanwhile in (d), 1SITR becomes excessively dissipative, resulting in a solution that is smoother than the exact one suggesting that significant damping at this discretization could affect amplitude accuracy.

Figure 9 illustrates the plot of the average error at different values of *dx* across a range of time step sizes. The damping characteristic of the 1SITR is greater than that of the 2SITR and can eliminate the oscillation of the solution much quicker than that of the 2SITR, which leads to a lower average solution error at a large time step. However, the rapid increase in solution dissipation results in an increase in the average error and thus lower accuracy at a smaller *dt*. In the case of a smaller *dx* 1SITR remains stable even at small *dt* value. Although 1SITR displays higher errors at smaller *dt* , it gradually outperforms GTDTM and 2SITR as *dt* continues to increase. This suggests that 1SITR is better for larger time steps and preserves consistent accuracy when a finer spatial grid *dx* = 0.24 is utilized. These quantitative findings reinforce that 1SITR achieves a more effective balance between damping and accuracy under appropriate discretization conditions.

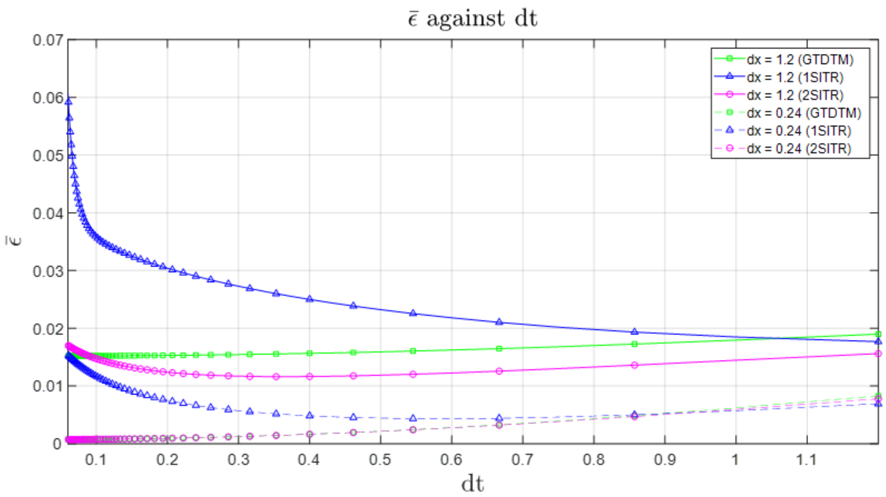

FIGURE 9. Plot of $\overline{\varepsilon}$ against dt at different values of *dx*

COMPUTATIONAL EFFICIENCY

Table 1 shows the computation time required by each method at larger values of *dx*. Among the three studied methods, the computation time required by 1SITR and 2SITR for the calculation of the solution is approximately two times longer than that of the GTDTM. Table 2 shows the computation time required by each method at a smaller *dx* value.

TABLE 1. Computation time at *dx* = 1.2

dt	Computation time (s)		
	GTDTM	1SITR	2SITR
0.06	0.1781	0.3504	0.3850
0.12	0.0768	0.2117	0.2018
0.60	0.0205	0.0458	0.0529
1.20	0.0124	0.0318	0.0307

TABLE 2. Computation time at *dx* = 0.24

dt	Computation time (s)		
	GTDTM	1SITR	2SITR
0.06	6.5633	12.8839	12.9375
0.12	3.2299	6.3945	6.4345
0.60	0.6396	1.3080	1.3435
1.20	0.3420	0.7109	0.7453

As the space step is reduced, the computation time required for solution calculation is significantly longer. The trend for the computation time with decreasing *dx* is similar to that for increasing *dt,* where both the 1SITR and 2SITR algorithms take approximately two times longer to generate the solution compared to the GTDTM algorithm. At any given condition of *dx* and *dt*, the computation time of 1SITR is almost equal to that of 2SITR in which 1SITR is slightly more efficient.

CONCLUSION

In this numerical study, FD schemes based on the generalized trapezoidal differencing time-marching (GTDTM) method, active one-step symmetrized implicit trapezoidal rule (1SITR) and active two-step symmetrized implicit trapezoidal rule (2SITR) are implemented to solve the linear advection equation. Several conclusions can be drawn from this study. First, for the conventional FD method, the GTDTM shows significant oscillation in the solution at large space steps, *dx* and time steps *dt*. In contrast, 1SITR and 2SITR can reduce oscillation due to their damping nature which can lead to an increase in the accuracy of the solution. Since the damping characteristic of the 1SITR is greater than that of the 2SITR, the former method can yield more accurate results at larger values of *dx* and *dt*.

Next, a decrease in parameters *dx* and *dt* leads to an increase in the damping characteristics of 1SITR and 2SITR which increases the accuracy of the methods. This occurs until a critical point where a further increase in the parameters leads to greater dissipation and leads to an increase in the average error.

Finally, the computational efficiency of 1SITR and 2SITR is less than that of the conventional GTDTM method due to the extra symmetrization step. However, since 1SITR and 2SITR are more accurate than GTDTM at larger values of *dx* and *dt*, it is practical to employ 1SITR and 2SITR at large space and time steps at which the computation time is reduced.

This study presents a unique contribution through the development and analysis of two symmetrized implicit trapezoidal rule methods which provide improved damping characteristics, allowing for more stable and accurate solutions even under coarse discretization settings. These methods tackle a significant issue in numerical simulations, particularly when traditional finite difference schemes struggle to preserve accuracy with larger step sizes. A limitation of the current study is its focus solely on linear and one-dimensional cases, which might limit its relevance to more intricate real-world situations. Future research could expand these methods to nonlinear partial differential equations and multidimensional contexts. Additionally, exploring the use of adaptive meshing or hybrid time-marching techniques might enhance computational efficiency.

ACKNOWLEDGEMENTS

This work was supported by Universiti Kebangsaan Malaysia and the Ministry of Higher Education under grant FRGS/1/2022/STG06/UKM/02/1, with additional funding from the Tabung Agihan Pelajar (TAP) scheme, University Kebangsaan Malaysia, which facilitated the study of symmetrized numerical methods in acoustic wave propagation.

DECLARATION OF COMPETING INTEREST

None

REFERENCES

Boom, P. D., & Zingg, D. W. 2018. Optimization of high-order diagonally-implicit Runge?Kutta methods. *Journal of Computational Physics* 371: 168–191.

Chan, R. P. K., & Gorgey, A. 2013. Active and passive symmetrization of Runge?Kutta Gauss methods. *Applied Numerical Mathematics* 67: 64–77.

Chan, R. P. K., & Razali, N. 2014. Smoothing effects on the IMR and ITR. *Numerical Algorithms* 65(3): 401–420. https://doi.org/10.1007/s11075-013-9779-7

Chang, H., Wang, F., Yue, X., Qiu, L., & Sun, L. 2023. A 2.5D generalized finite difference method for elastic wave propagation problems. *Mathematics* 11(10): 2321. https://doi.org/10.3390/math11102321

Chen, H., & Chen, Y. 2017. Modeling elastic wave propagation using K -Space Operator-based temporal high-order staggered-grid finite-difference method. *IEEE Transactions on Geoscience and Remote Sensing* 55(2): 801–815.

Chen, Y., & Deng, X. 2019. A stable dissipative compact finite difference scheme with global accuracy of ninth order. *Computers & Fluids* 185: 13–21.

Chen, L., Huang, J., Fu, L.-Y., Peng, W., Song, C., & Han, J. 2023. A Compact high-order finite-difference method with optimized coefficients for 2D acoustic wave equation. Remote *Sensing* 15(3): 604. https://doi.org/10.3390/rs15030604

Dahl, M. 2000. Workshop on Benchmark Problems. *Third Computational Aeroacoustics (C. A A)*.

Francesca, P., & Muhieldeen, M. W. 2020. Investigation on generalised trapezoidal differencing time-marching scheme for modelling of acoustical wave. *CFD Letters* 12(2): 11–21.

Gao, D., Zhang, P., Wang, L., Dai, Z., & Fang, Y. 2025. A novel high-order symmetric and energy-preserving continuous-stage Runge–Kutta–Nyström Fourier pseudo-spectral scheme for solving the two-dimensional nonlinear wave equation. *AIMS Mathematics* 10(3): 6764–6787. https://doi.org/10.3934/math.2025310

Hakroa, M. R., Almania, Z., Channab, M. A., & Jokhioc, J. 2024. Numerical modelling of matric suction in unsaturated soil under shallow foundation under varying soil and hydrological conditions. *Jurnal Kejuruteraan* 36(2): 569–580.

Hong, Q., Wang, C., Chen, Y., & Gong, Y. 2022. A novel class of energy-preserving Runge–Kutta methods for the Korteweg–de Vries equation. *Numerical Mathematics: Theory, Methods and Applications* 15(3): 768–792. https://doi.org/10.4208/nmtma.OA-2021-0172

Ismail, A., & Azadbakht, S. 2024. A comprehensive review of numerical simulation methods for hydraulic fracturing. *International Journal for Numerical and Analytical Methods in Geomechanics*.

Ketcheson, D. I. 2008. Highly Efficient Strong Stability-Preserving Runge?Kutta Methods with Low-Storage Implementations. *SIAM Journal on Scientific Computing* 30(4): 2113–2136.

Kosloff D. Tal-Ezer, H. 2010. *Acoustic and elastic numerical wave simulations by recursive spatial derivative operators*. Geophysics.

Lele, S. K. 1992. Compact finite difference schemes with spectral-like resolution. *Journal of Computational Physics* 103(1): 16–42.

Liu, Y., & Sen, M. K. 2013. Time?space domain dispersion-relation-based finite-difference method with arbitrary even-order accuracy for the 2D acoustic wave equation. *Journal of Computational Physics* 232(1): 327–345.

Nunez, L. Z., & Rao, M. M. 2013. Time-stepping beyond CFL: A locally one-dimensional scheme for acoustic wave propagation. In S. E. G. T. P. E. Abstracts (Ed.): *?3354* (p. 3350). Society of Exploration Geophysicists.

Ranocha, H. &. (2018). ffner, P. *L_2 L*, *75*(2).

Razali, N., & Chan, R. P. K. 2015. Implementation of symmetrizers in ordinary differential equations. *ANZIAM Journal* 55: 541.

Razali, N., Nopiah, Z. M., & Othman, H. 2018. Comparison of one-step and two-step symmetrization in the variable stepsize setting. *Sains Malaysiana* 47(11): 2927–2932. https://doi.org/10.17576/jsm-2018-4711-36

Ren, Z., & Sen, M. K. 2017. Modeling of the Acoustic Wave Equation by Staggered-Grid Finite-Difference Schemes with High-Order Temporal and Spatial Accuracy. *Bulletin of the Seismological Society of America* 107(5): 2160–2182.

Rona, A., & Pirozzoli, S. 2017. Optimised prefactored compact schemes for linear wave propagation phenomena. *Journal of Computational Physics* 328: 66–85.

Simillides, Y., Huthwaite, P., Kalkowski, M. K., & Lowe, M. J. 2024. A displacement-based finite element formulation for solving elastic wave problems in coupled fluid-solid media on a GPU. *Computers & Structures* 299: 107369.

Tan, S., & Huang, L. 2014. An efficient finite-difference method with high-order accuracy in both time and space domains for modelling scalar-wave propagation. *Geophysical Journal International* 197(2): 1250–1267.

Wang, E., & Liu, Y. 2019. Temporal high-order time?Space domain finite-difference methods for modeling 3D acoustic wave equations on general cuboid grids. *Pure and Applied Geophysics* 176(12): 5391–5414.

Wang, Z., & Chen, X. 2018. A new central compact finite difference scheme with high spectral resolution for acoustic wave equation. *Journal of Computational Physics* 366: 191–206.

Xu, S., & Liu, Y. 2018. 3D acoustic wave modeling with a time-space-domain temporal high-order finite-difference scheme. *Journal of Geophysics and Engineering* 15(5): 1963–1976.

Yang, L., & Liu, H. 2016. Optimal implicit staggered-grid finite-difference schemes based on the sampling approximation method for seismic modelling. *Geophysical Prospecting* 64(3): 595–610.

Yang, L., & Liu, H. 2017. Optimal staggered-grid finite-difference schemes based on the minimax approximation method with the Remez algorithm. *GEOPHYSICS* 82(1): T27–T42.

Zhang, Y., & Lu, S. W. 2007. Genetic algorithm in reduction of numerical dispersion of 3-D alternating-direction-implicit finite-difference time-domain method. *IEEE Transactions on Microwave Theory and Techniques* 55(5): 966–973.

Zhang, H., Yan, J., Qian, X., Gu, X., & Song, S. 2021. On the preserving of the maximum principle and energy stability of high-order implicit-explicit Runge–Kutta schemes for the space-fractional Allen–Cahn equation. *Numerical Algorithms* 88: 1309–1336. https://doi.org/10.1007/s11075-021-01077-x

Zhou, H., & Ortigosa, F. 2008. Construction and Analysis of an Optimized Compact Finite Difference Scheme for RTM. *70th EAGE Conference and Exhibition Incorporating SPE EUROPEC 2008*.

Zhou, H., & Zhang, G. 2011. Prefactored optimized compact finite-difference schemes for second spatial derivatives. *GEOPHYSICS* 76(5): WB87–WB95.